Supplement of Atmos. Chem. Phys., 15, 37–53, 2015
http://www.atmos-chem-phys.net/15/37/2015/
doi:10.5194/acp-15-37-2015-supplement

Atmospheric Chemistry and Physics
Open Access

Supplement of

Seasonal characteristics of fine particulate matter (PM) based on high-resolution time-of-flight aerosol mass spectrometric (HR-ToF-AMS) measurements at the HKUST Supersite in Hong Kong

Y. J. Li et al.

Correspondence to: C. K. Chan (keckchan@ust.hk)

1. Site location

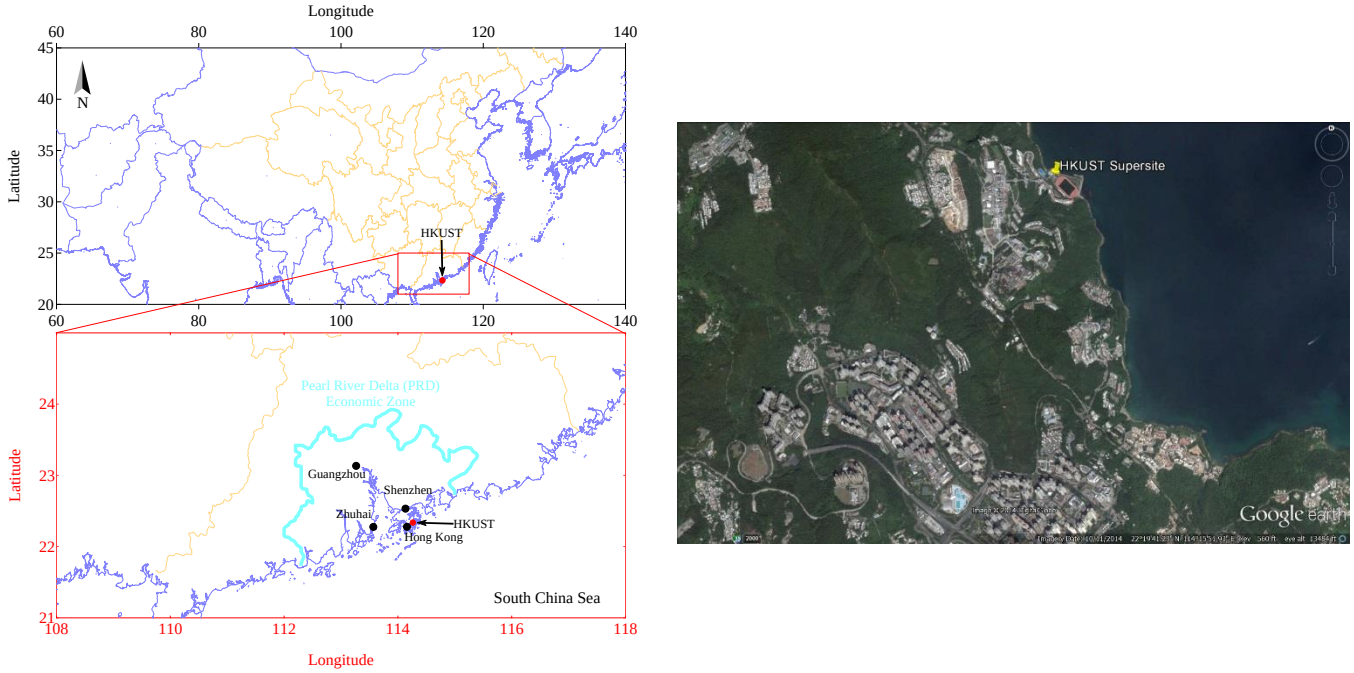

Figure S1 Location of the sampling site and its surrounding area.

2. Aerosol mass spectrometer (AMS) measurement

In pToF mode, the instrument performs particle sizing based on particle time-of-flight with the aid of a chopper and gives size-resolved chemical composition data in vacuum aerodynamic diameter (D_{va}) (DeCarlo et al., 2004;DeCarlo et al., 2006). In V mode, the shorter traveling path for ions in the ion time-of-flight (iToF) chamber gives a mass spectral resolving power of approximately 2000 and better sensitivity. In W mode, the mass spectral resolving power is approximately 4000 but the signal-to-noise ratio is lower. The instrument was operated alternately between the V+pToF combined mode and the W mode for 5 minutes each. The sampling inlet was shared by a few instruments and an extra pump was used to maintain the required flow rate (16.7 L/min) for the $PM_{2.5}$ size cut. A diffusion dryer (BMI, San Francisco, CA) was placed before the inlet of the HR-ToF-AMS to remove particulate water.

Ionization efficiency (IE) calibrations were performed weekly using size-selected ammonium nitrate particles (350 nm in mobility diameter, Dm). The flow rate of the inlet (~80 ml/min) and sizing (using standard PSL particles, Duke Scientific, Palo Alto, CA) were calibrated before and after the campaigns and negligible differences were observed. Frequent filtered periods (normally daily, maximum in three days) by putting an HEPA filter in front of the instrument inlet were performed for 30 to 60 min (3 to 6 data points for each mode). The results from the filter periods serve two purposes. First, the measured concentrations of all species in the "background" air can be used to calculate the campaign detection limits (CDLs) (Figures S2 and S3). Second, the intensities of ions affected by gaseous species (e.g., m/z 15, 16, 29, and 44) in the filter periods can be used to obtain more representative coefficients in the fragmentation table, which are essential for assigning signal intensities to particulate species. The correction factors (in addition to the original coefficients in the default fragmentation table) are given in Table S1 for all four months. In addition, the contribution of gaseous CO_2 to the variation in m/z 44 was corrected from the time-series of gaseous CO_2 concentrations (an additional season-dependent dynamic CO2_factor in Table S1) according to previous studies (Setyan et al., 2012;Collier and Zhang, 2013).

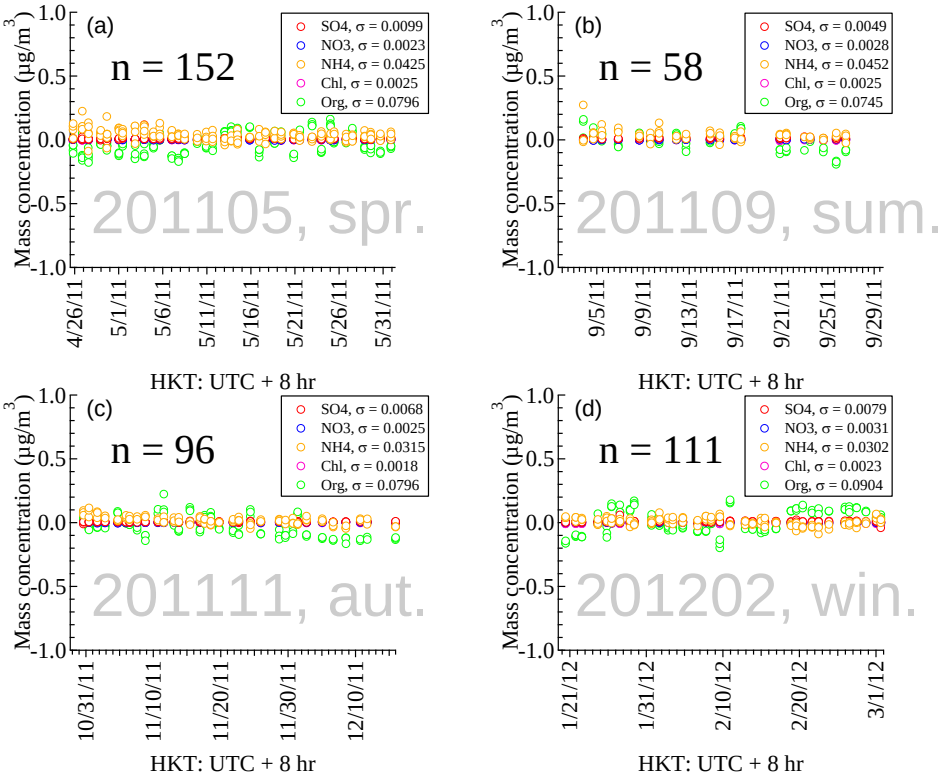

Figure S2 Mass concentrations of sulfate (SO4), nitrate (NO3), ammonium (NH4), chloride (Chl), and organics (Org) in the daily filter periods. In spring, one-hour filter periods were performed daily while in other months 30 min filter periods were performed.

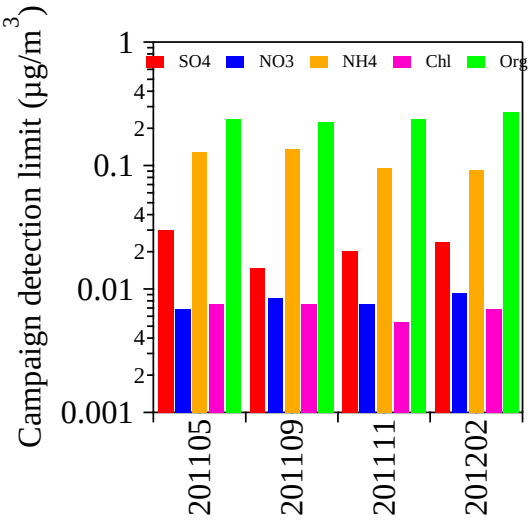

Figure S3 Four-month campaign detection limits (CDLs) of all five species as estimated by 3 times standard deviations of the concentration measured in filter periods.

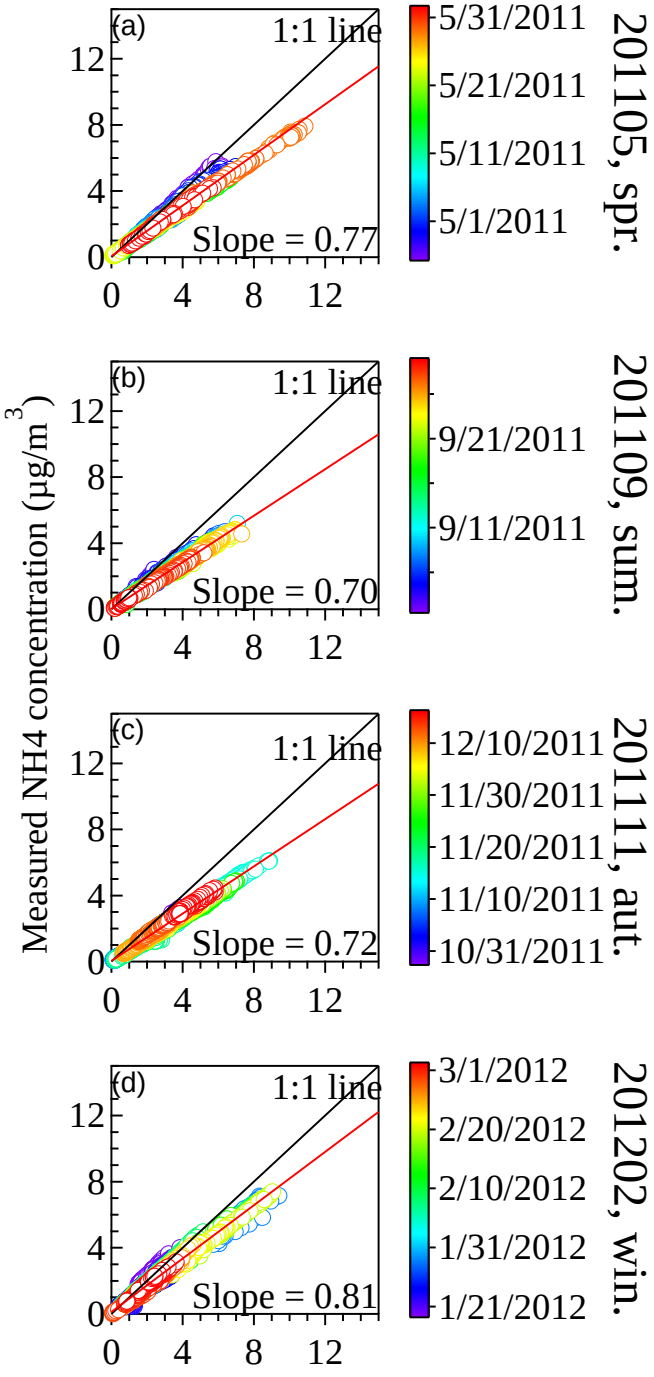

Figure S4 Measured vs predicted ammonium concentration in four seasons. Predicted ammonium concentrations are calculated by $NH_{4,p} = 18 \times (2 \times SO_{4,m}/96 + NO_{3,m}/62 + Chl_m/35.5)$, where "p" denotes "predicted" and "m" denotes "measured".

3. Modification to fragmentation table

Table S1 Additional coefficients used to correct the ion contributions to organic signals beyond the default fragmentation table. CO_2_factor is the correction factor of gaseous CO_2 contribution to m/z 44, which was computed by the individual CO_2 concentrations (matching with AMS time steps) divided by the average CO_2 concentration in a monthly campaign.

	m/z 15	m/z 16	m/z 29	m/z 44
201105, spring	0.87	1.06	0.80	0.90 × CO_2_factor
201109, summer	0.90	1.11	0.77	0.85 × CO_2_factor
201111, autumn	0.85	1.04	0.72	0.80 × CO_2_factor
201202, winter	0.79	1.04	0.64	0.70 × CO_2_factor

4. Non-refractory PM_1 measured by AMS in Asia

Table S2 Summary of AMS measurements in Asia.

Location	Acronym[a]	Sampling period	Characteristic	Inorganics			Organics		Elemental analysis		Reference	AMS[f]
				Sulfate	Nitrate	Ammonium	POA[b]	OOA[c]	O:C[d]	H:C[e]		
Eastern Asia	–	Apr., 2001	ground	6.08 ± 1.80	2.31 ± 1.45	2.03 ± 1.30	7.13 ± 3.88		–	–	(Bahreini et al., 2003)	(1)
			< 100 m	3.01 ± 2.08	0.97 ± 0.75	1.32 ± 0.34	4.46 ± 2.70		–	–		
			100 - 1000 m	2.49 ± 1.74	1.13 ± 0.54	1.06 ± 0.48	6.06 ± 3.78		–	–		
			1000 - 3000 m	2.34 ± 2.61	0.55 ± 0.50	1.58 ± 1.20	3.65 ± 2.47		–	–		
			> 3000 m	1.41 ± 1.11	0.41	3.38	2.62 ± 2.36		–	–		
Jeju Island, Korea	JJK	Apr., 2001	remote	3.09 ± 1.74	0.51 ± 0.55	1.48 ± 1.45	3.49 ± 3.14		–	–	(Topping et al., 2004)	(1)
Fukue, Japan	FKJ	Mar. and Apr., 2003	remote	4.80	0.56	1.57	5.03		–	–	(Takami et al., 2005)	(1)
Okinawa, Japan	–	Mar., 2005	remote	6.37 ± 4.30	–	1.25 ± 0.94	2.16 ± 1.60		–	–	(Takami et al., 2007)	(1)
Wakayama, Japan	–	Aug., 2010	forest	1.6	–	0.5	1.8		–	–	(Han et al., 2014)	(3)
Changdao, China	CDC	Mar. – Apr., 2011	receptor	8.3 ± 7.3	12.2 ± 12.0	6.5 ± 6.0	4.4	9.4	0.59 ± 0.10	1.33 ± 0.07	(Hu et al., 2013)	(3)
Qingyuan, China	QYC	Jul., 2006	rural/SE-south	13.4 ± 8.6	1.3 ± 1.4	4.1 ± 2.7	12.8 ± 7.8		–	–	(Xiao et al., 2011)	(1)
			rural/southwest	10.1 ± 3.8	1.0 ± 0.5	3.3 ± 1.5	15.7 ± 6.3		–	–		
			rural/north	14.8 ± 9.6	1.8 ± 2.0	5.2 ± 3.9	18.7 ± 10.9		–	–		
			rural/east	4.7 ± 3.7	1.4 ± 1.8	2.0 ± 1.8	7.3 ± 5.3		–	–		
Kaiping, China	KPC	Oct. – Nov., 2008	rural	11.1	3.5	4.6	2.7	8.5	0.47 ± 0.07	1.48 ± 0.08	(Huang et al., 2011)	(3)
Yufa, China	YFC	Aug. – Sep., 2006	suburban	8.20 ± 7.46	2.88 ± 2.51	4.07 ± 3.23	10.83 ± 7.79		–	–	(Gunthe et al., 2011)	(1)
Jiaxing, China	JXC	Jun. – Jul., 2010	suburban	8.3	5.9	4.1	3.3	7.2	–	–	(Huang et al., 2013)	(3)
		Dec., 2010		7.1	7.5	4.9	5.0	7.7	–	–		
Hong Kong, China	HKC	May, 2011	suburban	7.4 ± 4.5	0.6 ± 0.7	2.3 ± 1.4	0.8	3.2	0.38 ± 0.11	1.35 ± 0.11	This study	(3)
		Sep., 2011		8.7 ± 3.8	0.4 ± 0.4	2.4 ± 1.0	0.7	3.4	0.52 ± 0.12	1.36 ± 0.11		
		Nov., 2011		7.1 ± 3.7	0.7 ± 0.5	2.1 ± 1.1	0.8	5.2	0.42 ± 0.08	1.39 ± 0.07		
		Feb., 2012		6.2 ± 3.2	1.6 ± 1.4	2.4 ± 1.2	1.0	4.1	0.43 ± 0.07	1.40 ± 0.06		
Heshan, China	HSC	Nov., 2010	urban outflow	10.0	6.2	4.6	5.6	11.8	0.40 ± 0.06	1.49 ± 0.07	(Gong et al., 2012)	(3)
Tokyo, Japan	TKJ	Feb., 2003	urban	$2.5^{3.6}_{1.5}$	$3.1^{8.7}_{0.8}$	$2.2^{4.7}_{1.1}$	$6.7^{10.5}_{3.4}$		–	–	(Takegawa et al., 2006)	(1)
		Jul. – Aug., 2003		$3.2^{4.7}_{2.0}$	$1.0^{2.3}_{0.4}$	$1.8^{2.7}_{1.0}$	$5.7^{8.9}_{3.5}$		–	–		
		Sep. – Oct., 2003		$1.8^{2.6}_{1.1}$	$1.0^{2.9}_{0.5}$	$1.3^{2.0}_{0.7}$	$7.1^{10.3}_{4.6}$		–	–		
		Jan. – Feb., 2004		$1.7^{2.5}_{1.2}$	$2.8^{5.6}_{1.3}$	$2.3^{3.9}_{1.4}$	$5.8^{9.4}_{3.7}$		–	–		
Beijing, China	BJC	Jul., 2006	urban	20.3 ± 11.6	17.3 ± 13.2	13.1 ± 7.4	11.0	17.1	–	–	(Sun et al., 2010)	(1)
Beijing, China	BJC	Jul. – Sep., 2008	urban	16.8	10.0	10.0	10.2	13.7	–	–	(Huang et al., 2010)	(3)
Shenzhen, China	SZC	Oct. – Dec., 2009	urban	10.9	4.5	4.5	8.2	9.5	0.30 ± 0.06	1.63	(He et al., 2011)	(3)
Shanghai, China	SHC	May – Jun., 2010	urban	9.7	4.8	3.9	2.0	6.4	0.31	1.64	(Huang et al., 2012)	(3)
Tianjin, China	TJC	Sep., 2010	urban	14.4	16.2	13.6	15.7		–	–	(Zhang et al., 2012)	(2)
Beijing, China	BJC	Jun. – Aug., 2011	urban	9.0	12.4	8.0	7.1	12.7	–	–	(Sun et al., 2012)	(4)
Gwangju, Korea	GJK	Sep., 2011	urban	1.75 ± 0.85	0.62 ± 0.27	1.07 ± 0.63	4.70 ± 1.81		–	–	(Park et al., 2012)	(1)
		Dec., 2011		1.90 ± 0.57	2.45 ± 1.03	1.70 ± 0.67	6.31 ± 1.77		–	–		
Beijing, China	BJC	Nov., 2011 – Jan., 2012	urban	9.3	10.9	8.6	23.7	10.7	–	–	(Sun et al., 2013)	(4)
Beijing, China	BJC	Jan., 2013 (unpolluted)	urban	3.5	1.4	1.4	5.9	3.2	0.34 ± 0.08	1.44 ± 0.05	(Zhang et al., 2014)	(3)
		Jan., 2013 (polluted)		39.2	22.4	15.4	21.2	36.2				

[a]: Acronyms of the sampling locations used in Figure 2. [b]: Primary organic aerosols (POA) include one or more of hydrocarbon-like organic aerosols (HOA), cooking organic aerosols (COA), biomass burning organic aerosols (BBOA), and coal-combustion organic aerosols (CCOA); [c]: Oxygenated organic aerosols (OOA) include either OOA I and OOA II or low-volatility oxygenated organic aerosols (LVOOA) and semi-volatile oxygenated organic aerosols (SVOOA); [d]: oxygen-to-carbon atomic ratio (O:C); [e]: hydrogen-to-carbon atomic ratio (H:C); [f]: Type of AMS, (1) is Quadrople AMS (Q-AMS), (2) is compact Time-of-Flight AMS (c-ToF-AMS), (3) is High-Resolution Time-of-Flight AMS (HR-ToF-AMS), (4) is Aerosol Chemical Speciation Monitor (ACSM).

5. PMF diagnostics and evaluation

Figures S5 to S8 are the diagnostic plots for the PMF (with HR data) solutions with the original 7 or 8 factors for the four campaigns. Panels (a) and (b) are Q/Q_{exp} values as functions of factor number and fPeak value, respectively. Panel (c) is the mass fraction of each factor (with factor number of 7 or 8) as a function of fPeak value. Panel (d) is the correlation coefficient (R) of time series (tseries) and mass spectra (profile) for each factor pair (e.g., 1_2 represents factors 1 and 2 etc.). Panel (e) shows the measured total organic concentration and the "reconstructed" total organic concentration by all the factors (with factor number of 7 or 8). The "residual" organic concentration is the difference of the two, as shown in Panel (f). Panels (g) and (h) are the Q/Q_{exp} values for the time series and mass spectra, respectively. Panel (i) is the box-whisker plot for the scaled residual for the mass spectra. To assess the uncertainty of the factor time series and mass spectra, bootstrapping was performed for 100 runs with the chosen factor number, and it is shown with the average time series and mass spectral profile with one standard deviation in Figure S9.

Figures S10-S17 show the evaluation plots for both the original factor number (7 or 8) and the combined factors (4 factor), with concentration time series plotted with external tracer components (left column), high resolution mass spectra with elemental analysis results (second column), and correlation with "standard" mass spectra (second last column for UMR mass spectra and last column for HR mass spectra). Factor combination was done by evaluating the original factors to see whether they have similar concentration time series with the external tracer species or similar mass spectral

profile with the "standard" mass spectra. If so, the factors were combined to a single factor representing the overall feature of the new factor. Concentration time series combination is a simple summation of each sub-factors. Mass spectral combination is the average mass spectrum of the sub-factors. Table S3 shows the improvements of correlations in concentration time series of the combined factors with those of the external tracer species and in mass spectra with the "standard" spectra.

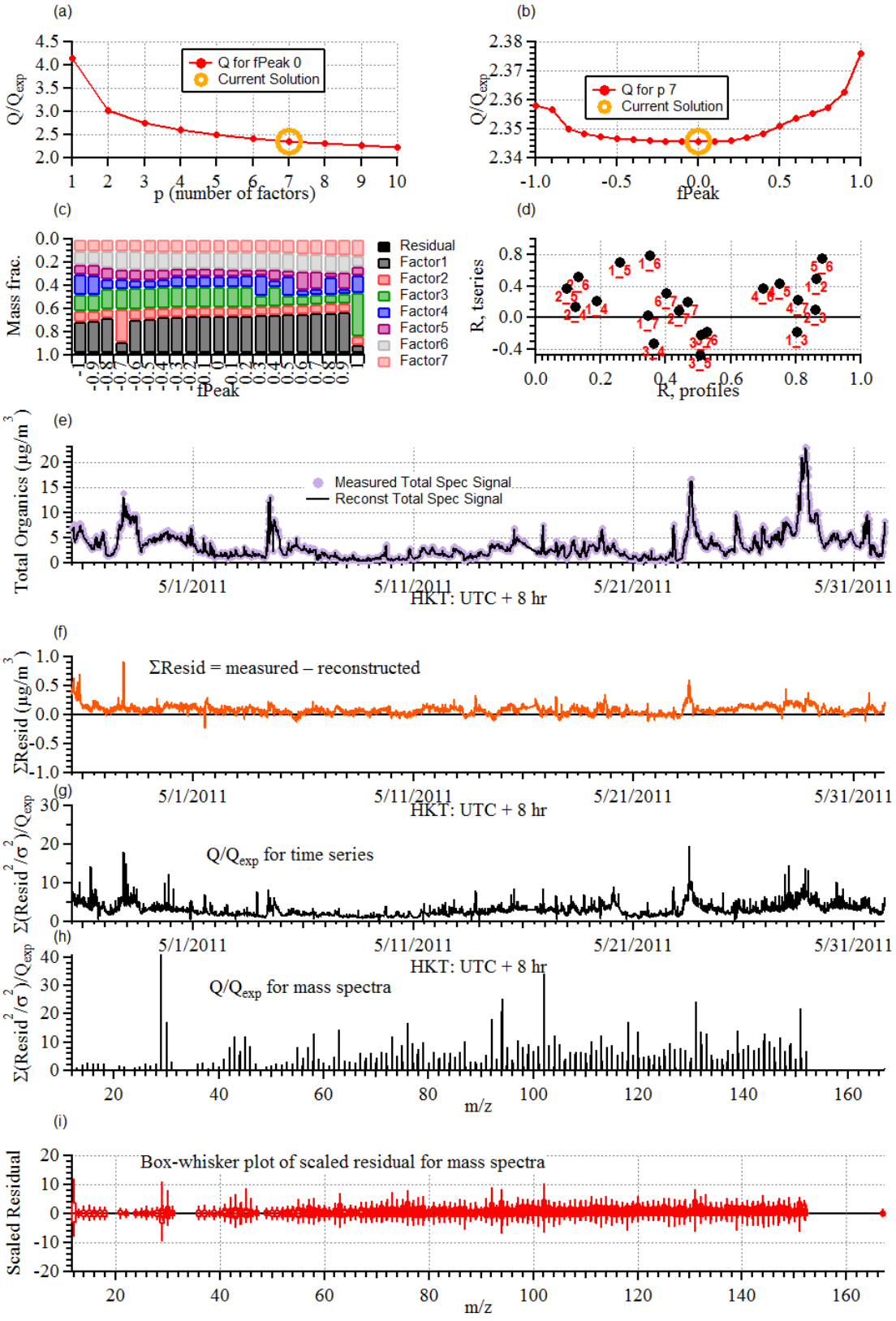

Figure S5 Diagnostic plot for 201105, spring.

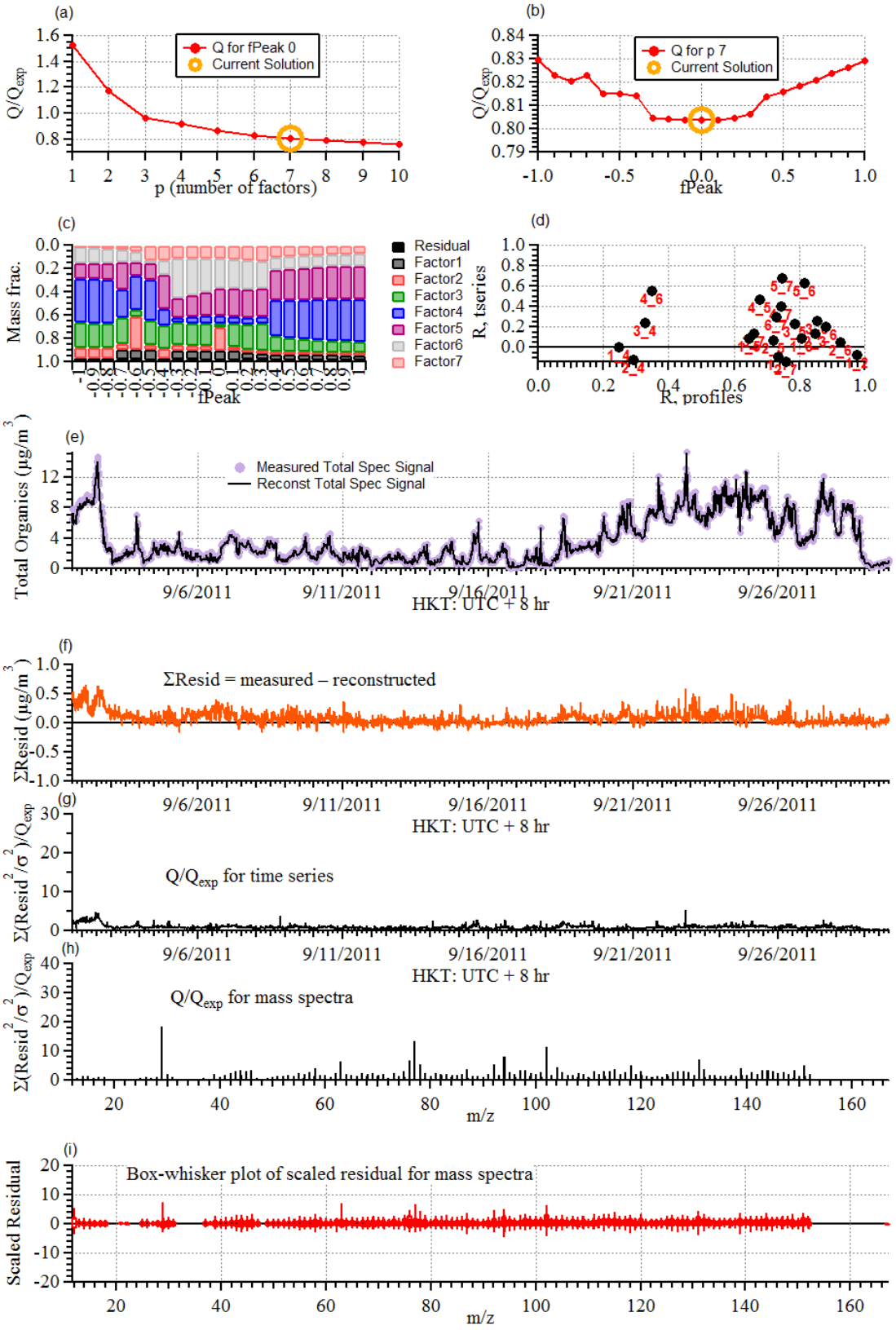

Figure S7 Diagnostic plot for 201109, summer.

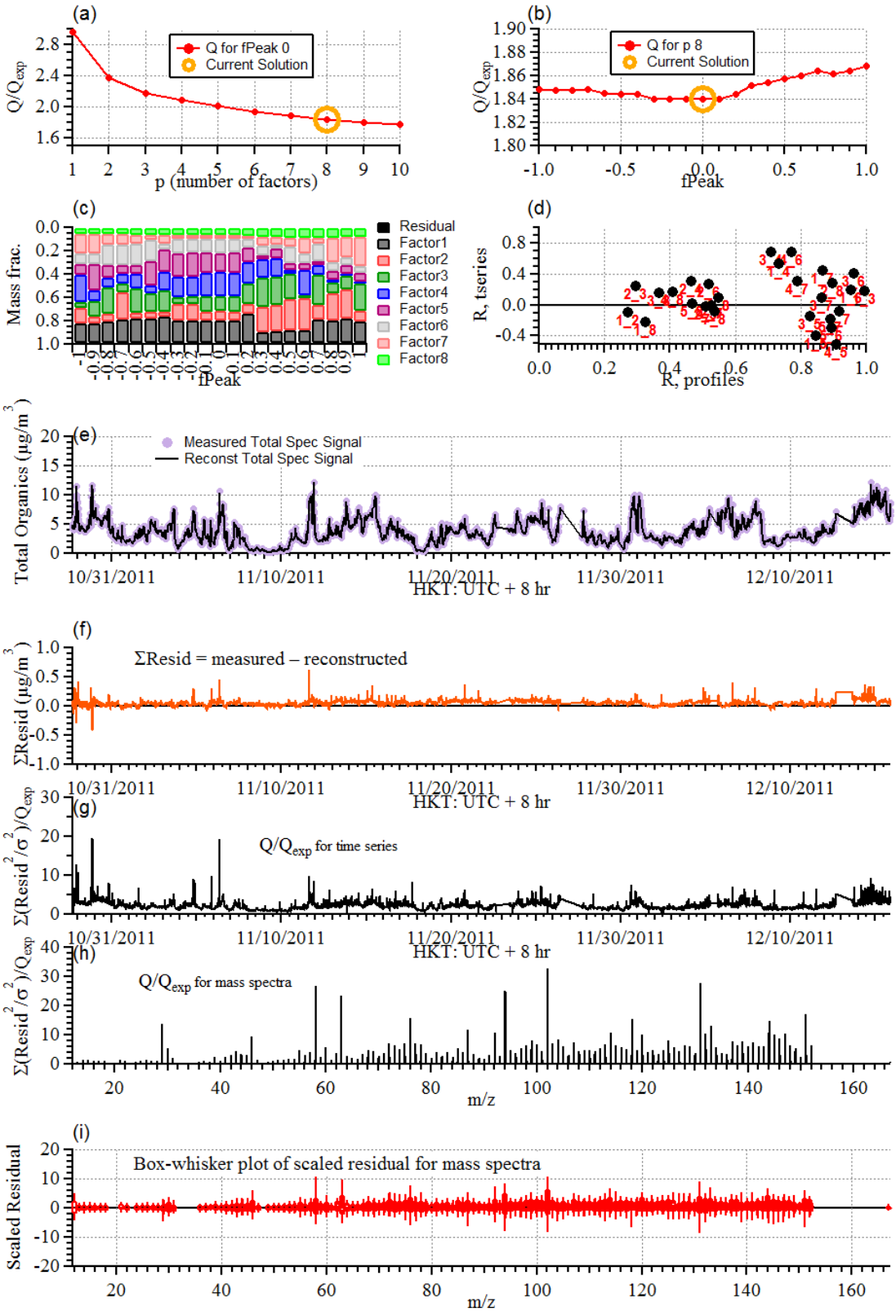

Figure S7 Diagnostic plot for 201111, autumn.

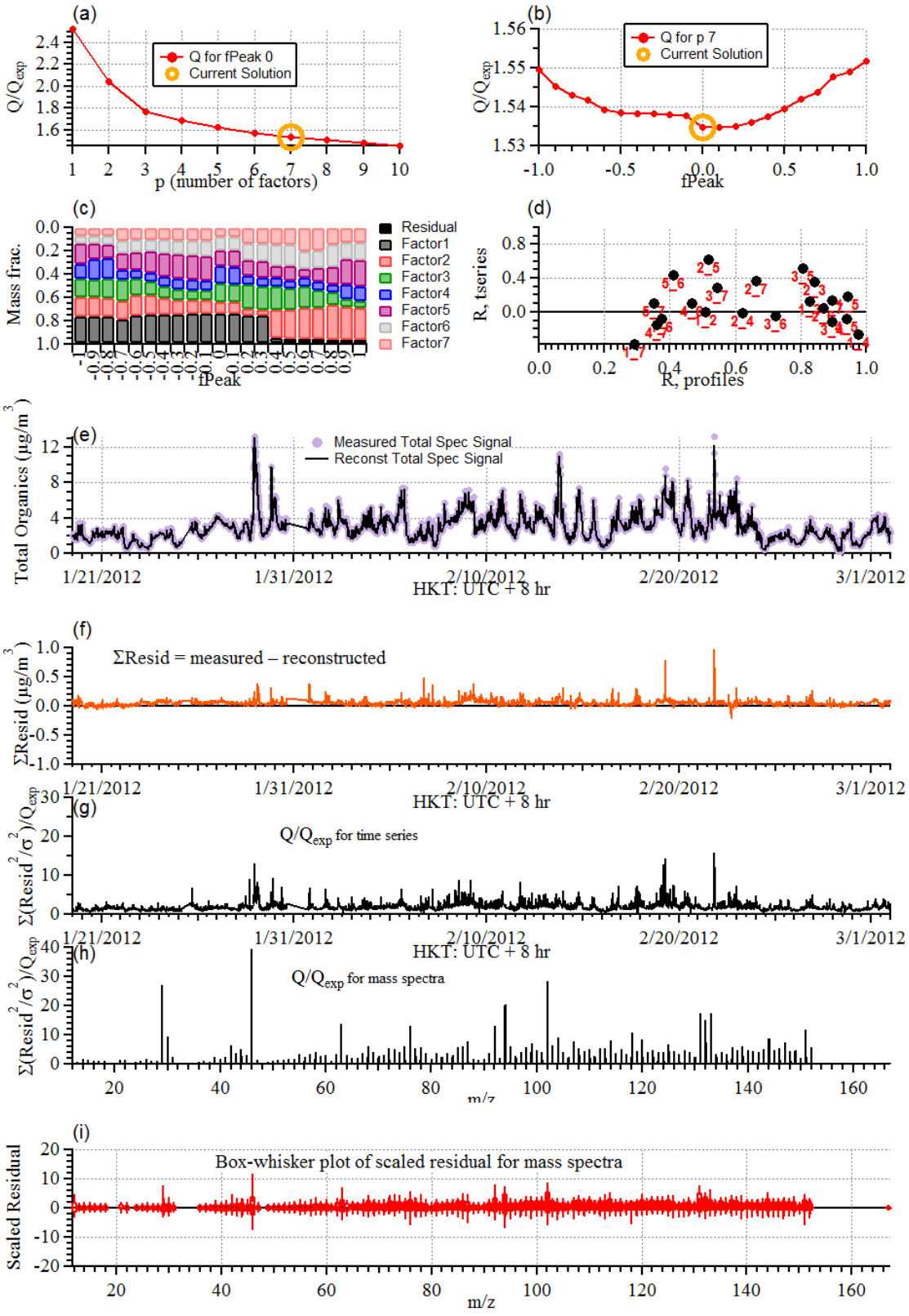

Figure S8 Diagnostic plot for 201202, winter.

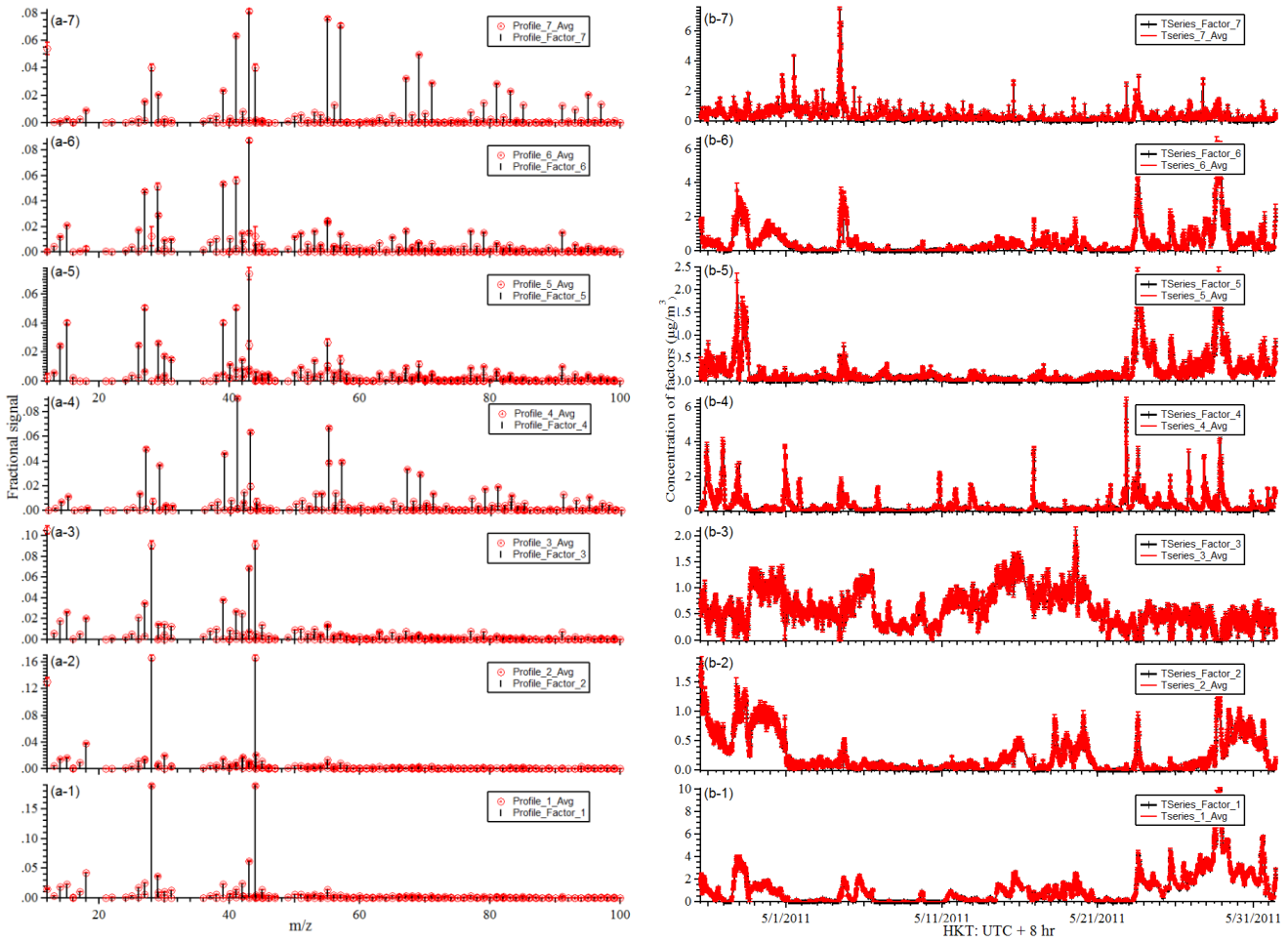

Figure S9 Example of bootstrapping plot (201105, spring). "Profile_x_Avg" is the average with standard deviation (from 100 bootstrapping runs) of the mass spectra for each Factor (x represents Factor 1 to 7). "Profile_Factor_x" represents the stick mass spectra for each Factor x. "TSeries_Factor_x" is the time series of concentration of each Factor x, while "Tseries_x_Avg" is the concentration time series with standard deviation (from 100 bootstrapping runs).

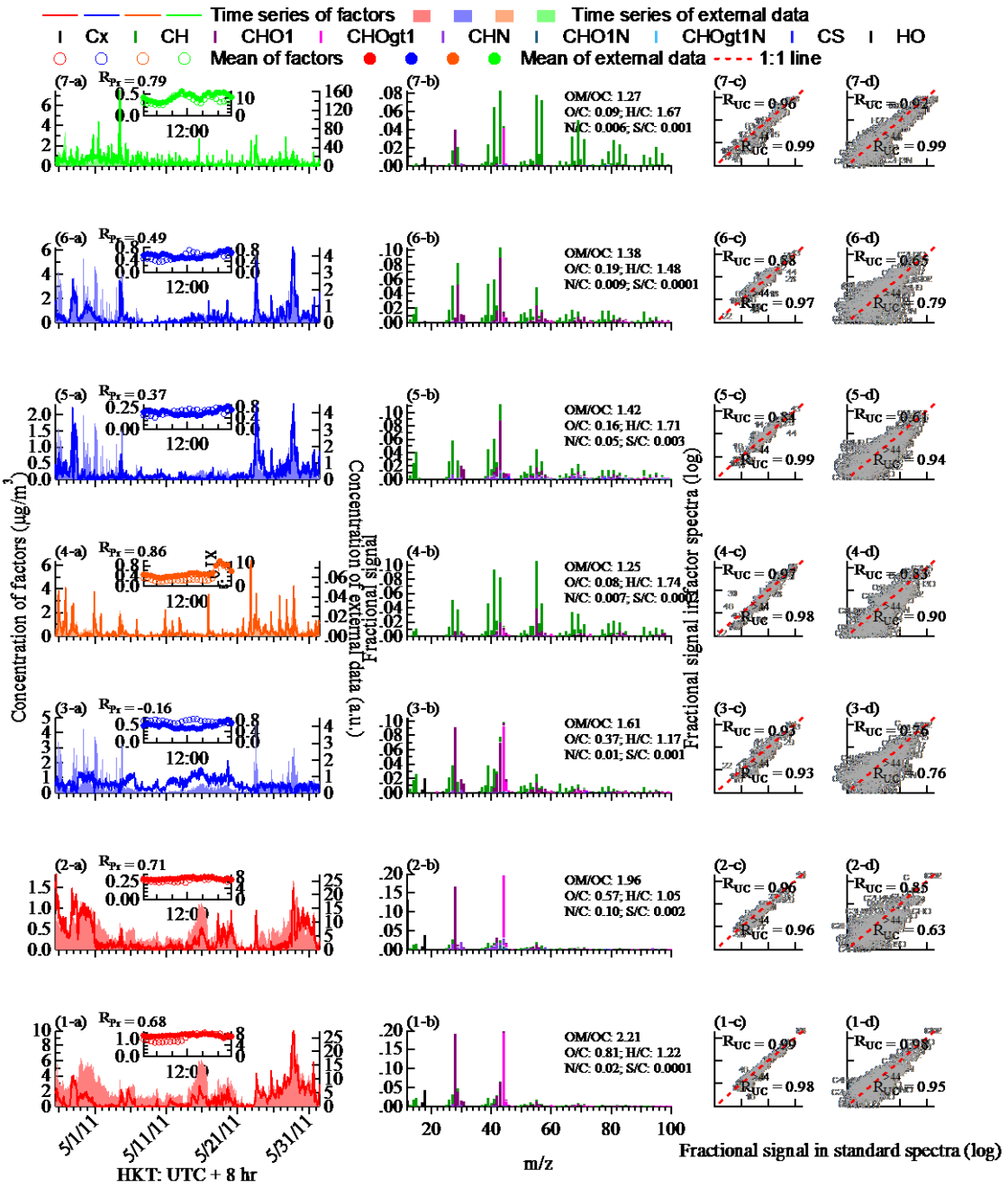

Figure S10 Original 7-factor solution for 201105, spring. x-a: concentration time series of each Factor x. The inserts of panels x-a are the diurnal patterns of each Factor. x-b: high-resolution mass spectra of each factor with elemental analysis results (OM/OC is organic matter to organic carbon ratio, O/C is oxygen-to-carbon atomic ratio, H/C is hydrogen-to-carbon atomic ratio, N/C is nitrogen-to-carbon atomic ratio, and S/C is sulfur-to-carbon atomic ratio). x-c: correlation of unit-mass-resolution mass spectra of each Factor with standard unit-mass-resolution mass spectra. x-d: correlation of high-resolution mass spectra of each Factor with standard high-resolution mass spectra. R_{Pr} is the Pearson's R, R_{UC} is the un-centered R for whole mass spectra, and $R_{UC}^{>44}$ is the un-centered R for ions with m/z > 44.

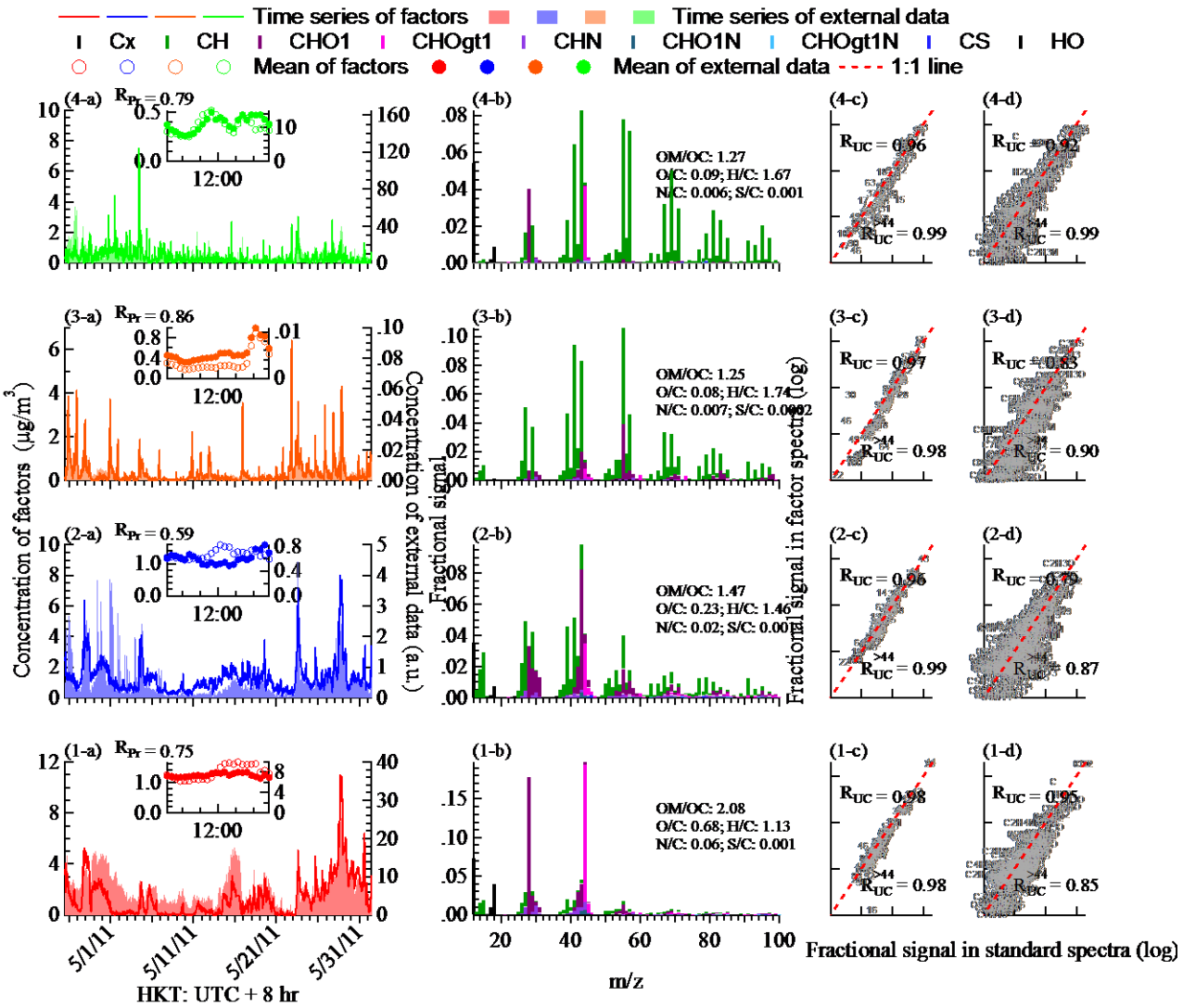

Figure S11 Combined 4-factor solution for 201105, spring. See caption of Figure S10 for detailed explanation of the legends.

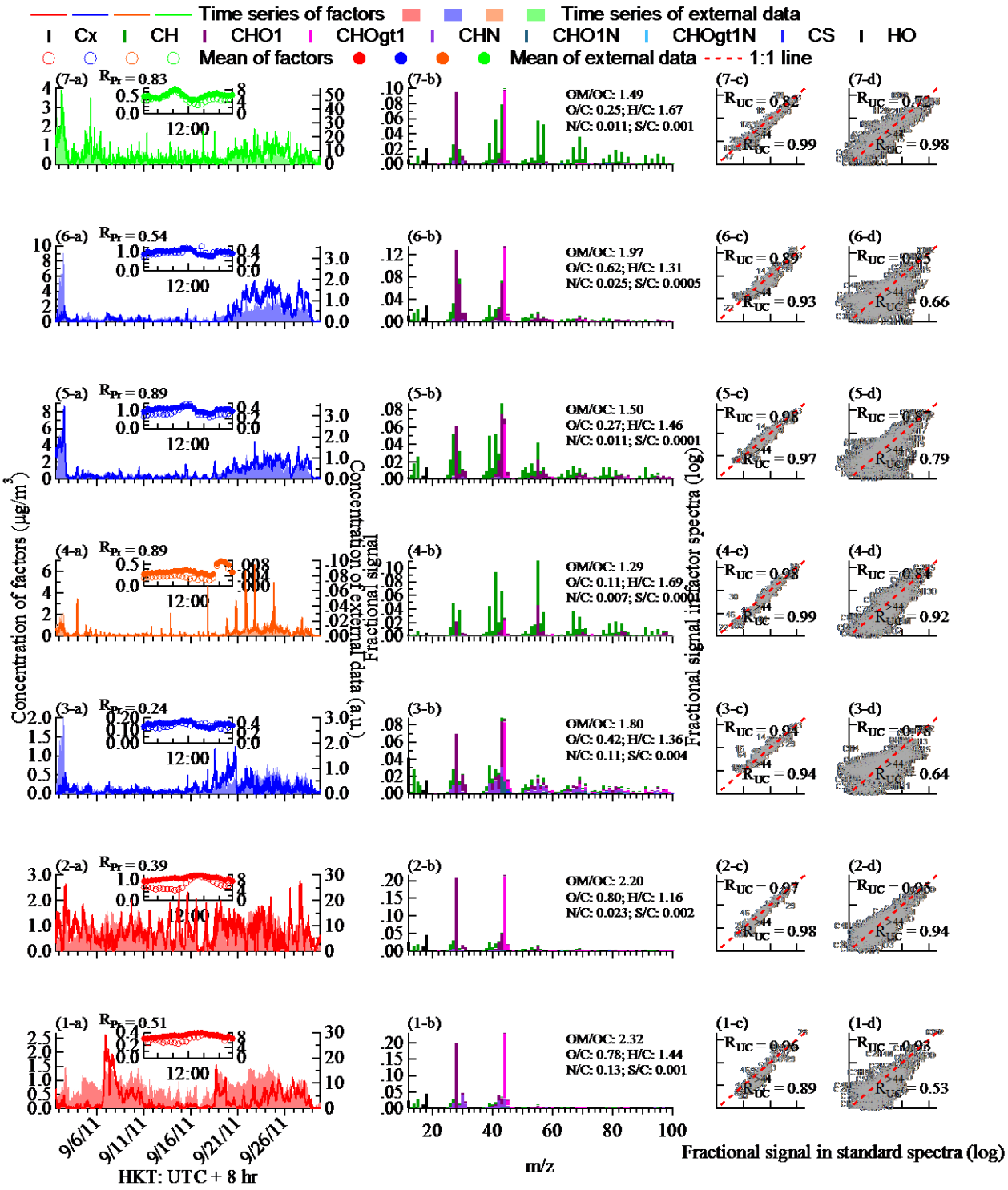

Figure S12 Original 7-factor solution for 201109, summer. See caption of Figure S10 for detailed explanation of the legends.

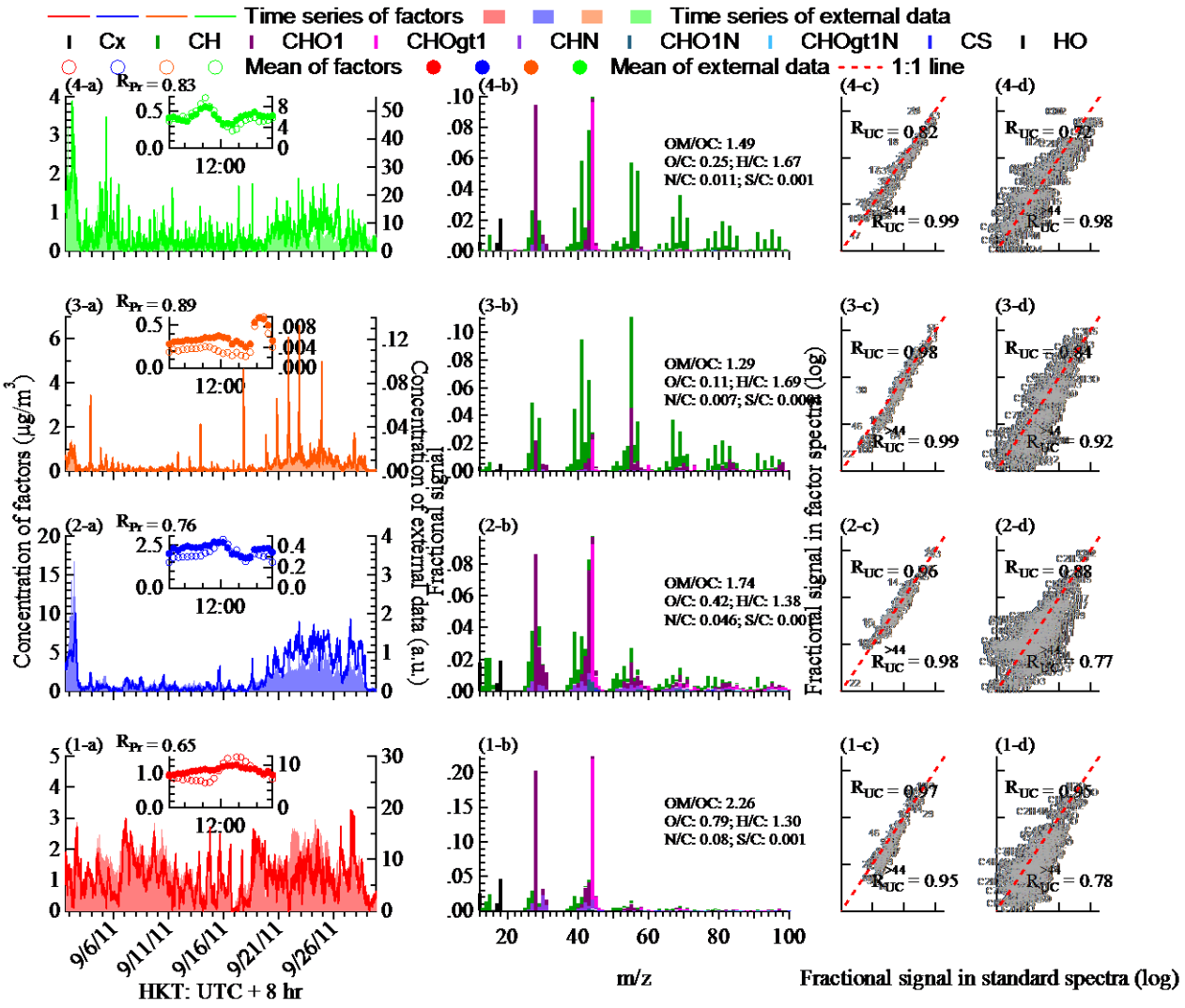

Figure S13 Combined 4-factor solution for 201109, summer. See caption of Figure S10 for detailed explanation of the legends.

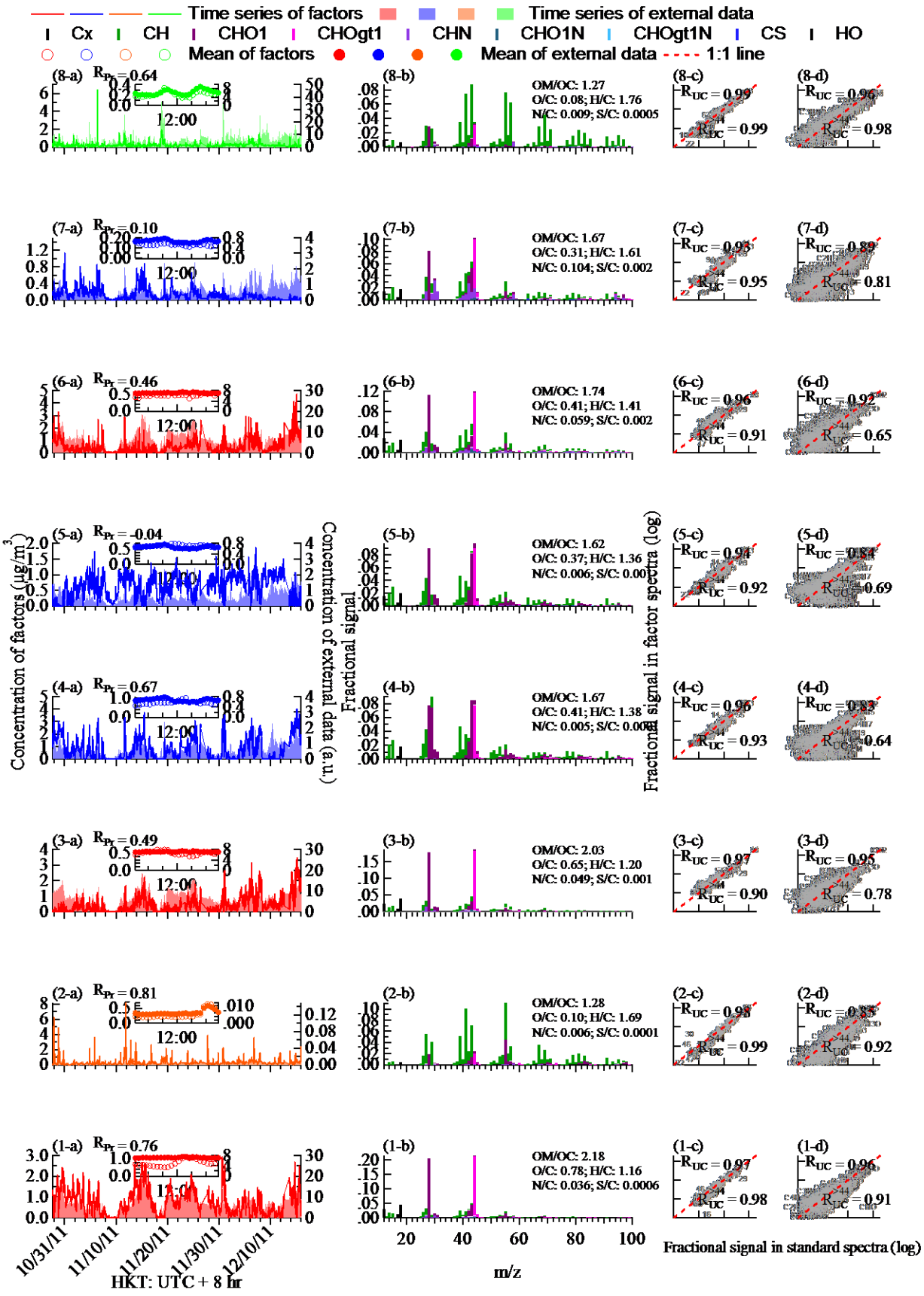

Figure S14 Original 8-factor solution for 201111, autumn. See caption of Figure S10 for detailed explanation of the legends.

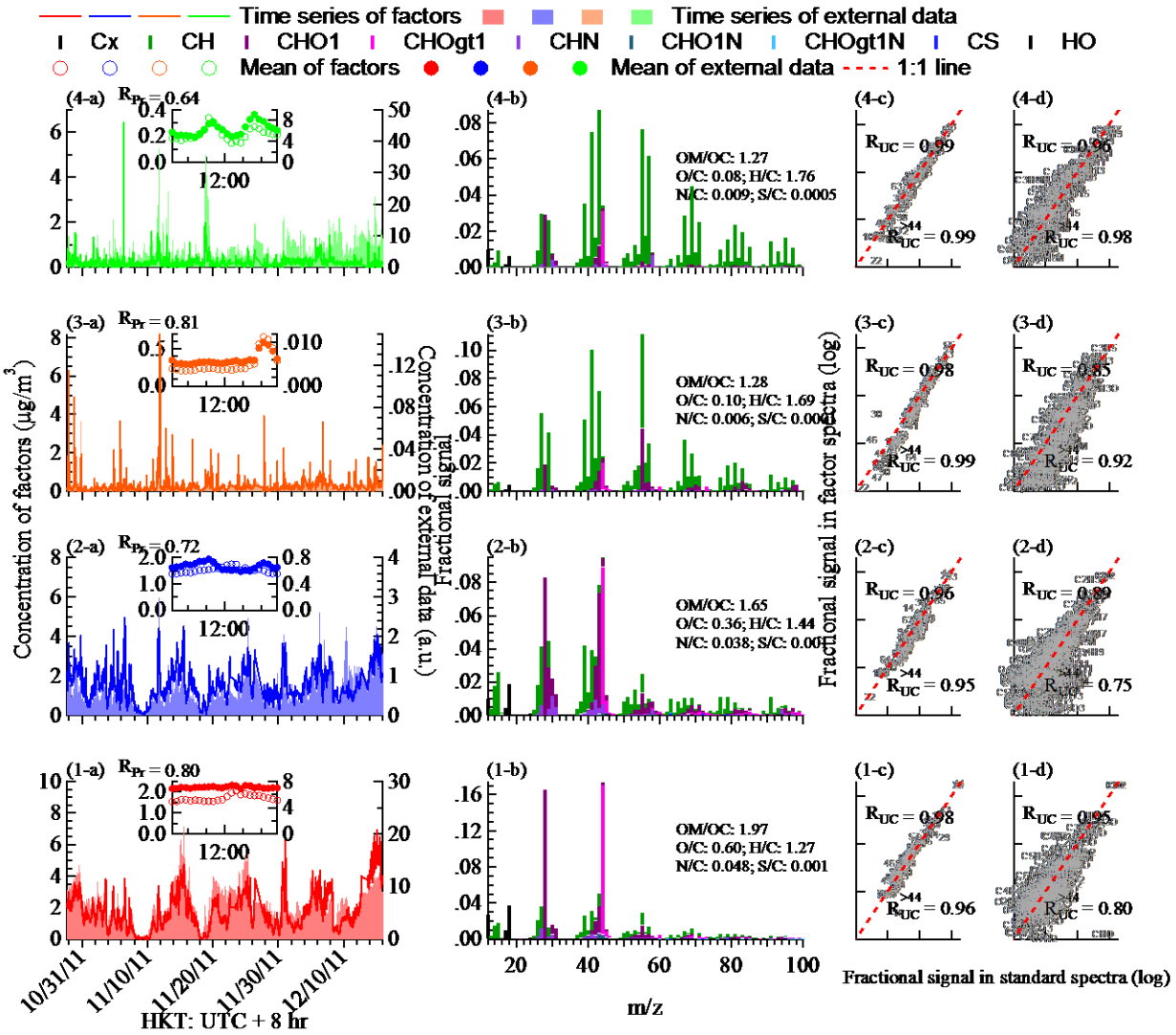

Figure S15 Combined 4-factor solution for 201111, autumn. See caption of Figure S10 for detailed explanation of the legends.

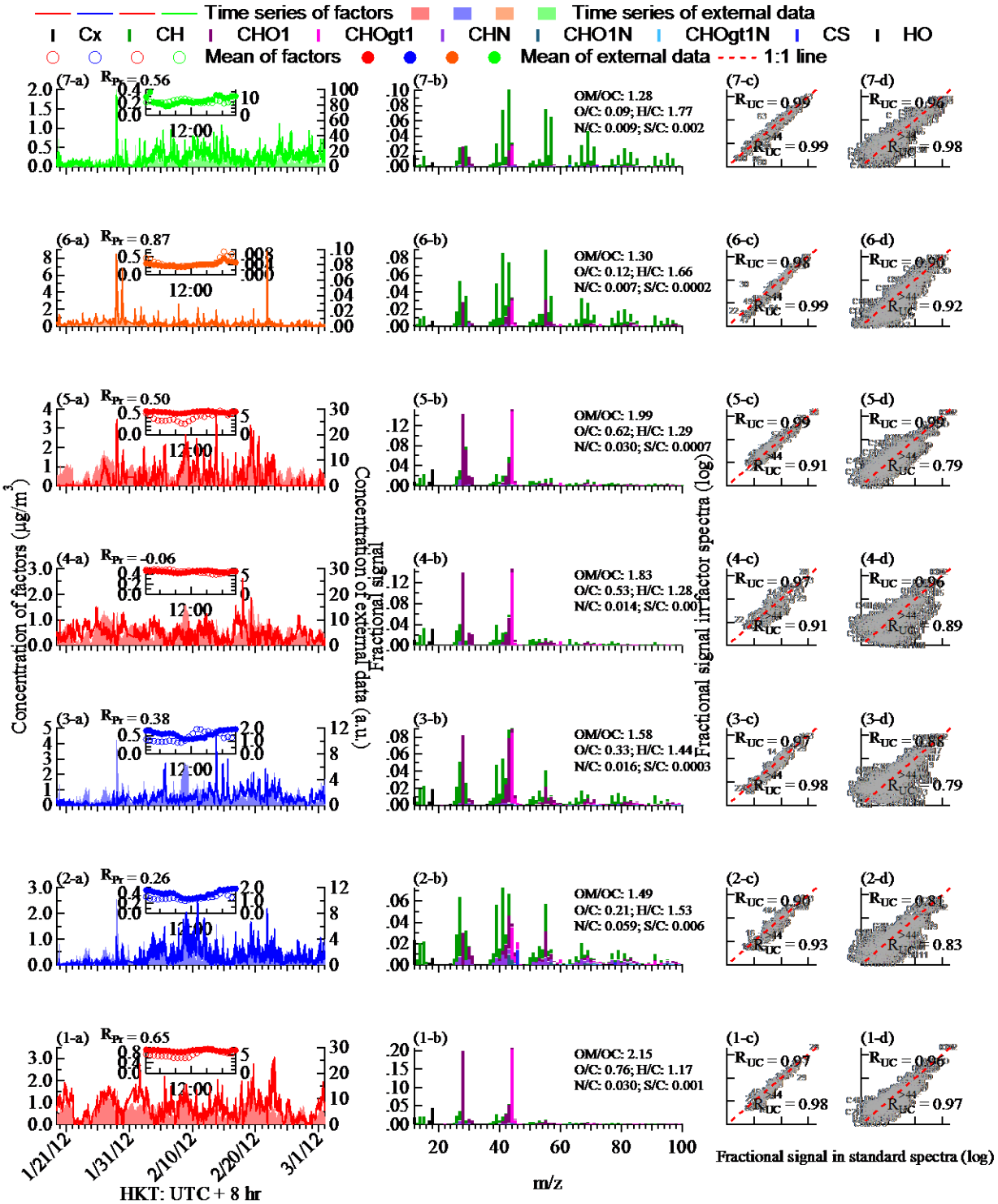

Figure S16 Original 7-factor solution for 201202, winter. See caption of Figure S10 for detailed explanation of the legends.

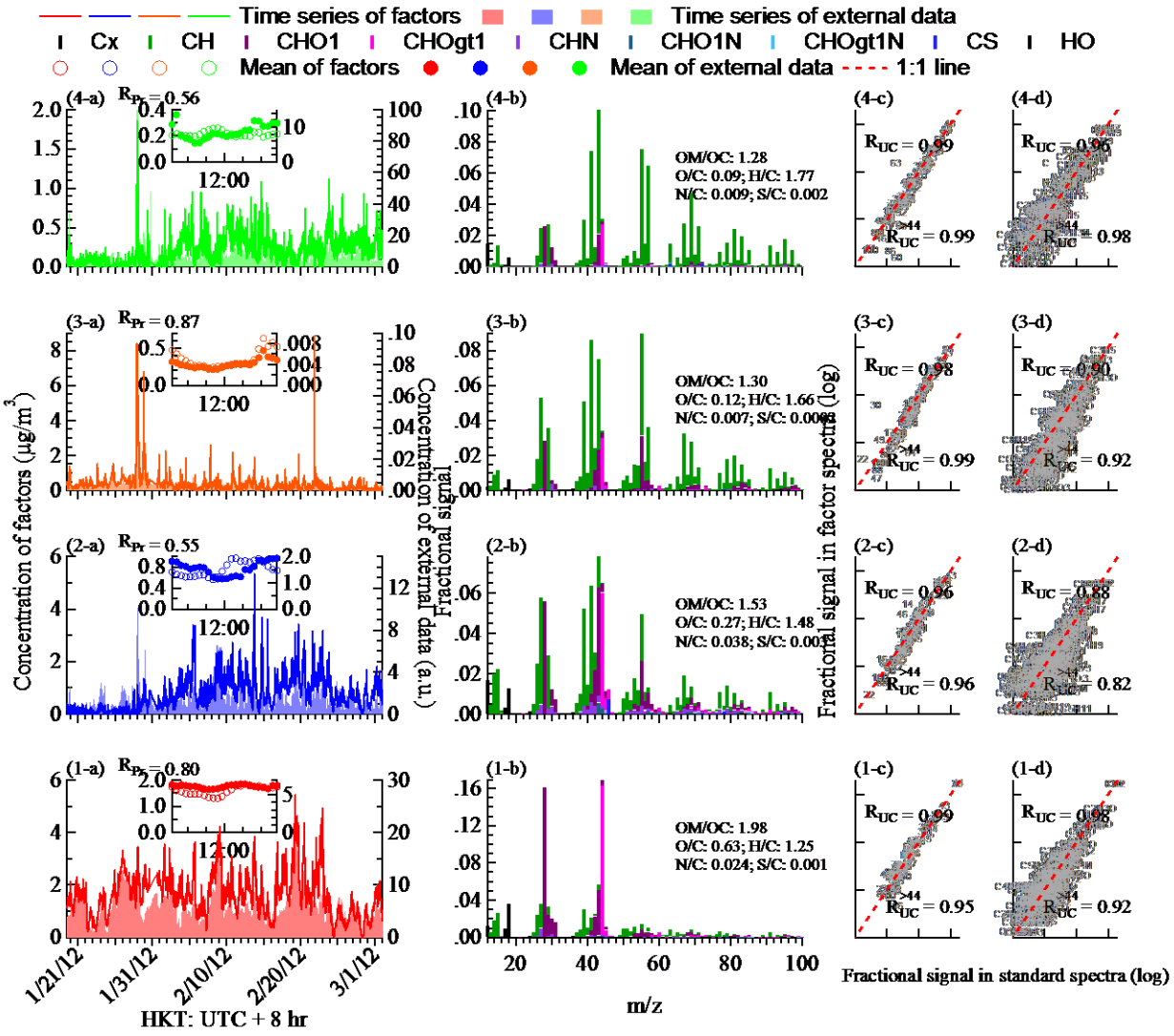

Figure S17 Combined 4-factor solution for 201202, winter. See caption of Figure S10 for detailed explanation of the legends.

Table S3 Summary of correlation coefficients of time series (TS) with external data and mass spectra (MS) with those in the literature. UMR is for unit-mass-resolution spectra and HR is for high-resolution mass spectra. Fx (x = 1 to 8) is the Factor number. "3ions" means the three ions ($C_5H_8O^+$, $C_6H_{10}O^+$, and $C_7H_{12}O^+$) used as tracers for COA. NOx is NO + NO_2. R_{Pr} is the Pearson's R, R_{UC} is the un-centered R for whole mass spectra, and $R_{UC}^{>44}$ is the un-centered R for ions with m/z > 44.

Color code	R_{Pr}	<0.4	0.4< <0.6	0.6< <0.8	>0.8								Color code	R_{UC}	$R_{UC}^{>44}$	<0.7	0.7< <0.8	0.8< <0.9	>0.9		
Season	Factor	TS	R_{Pr}	Factor	TS	R_{Pr}	Factor	MS	UMR		HR		Factor	MS	UMR		HR				
									R_{UC}	$R_{UC}^{>44}$	R_{UC}	$R_{UC}^{>44}$			R_{UC}	$R_{UC}^{>44}$	R_{UC}	$R_{UC}^{>44}$			
Spring, 201105	F1	SO4	0.68	F1	SO4	0.75	F1	LVOOA	0.99	0.98	0.98	0.95	F1	LVOOA	0.98	0.98	0.95	0.85			
	F2	SO4	0.71	F2	NO3	0.59	F2	LVOOA	0.96	0.96	0.85	0.63	F2	SVOOA	0.96	0.99	0.79	0.87			
	F3	NO3	-0.16	F3	COA_3ions	0.86	F3	SVOOA	0.93	0.93	0.76	0.76	F3	COA	0.97	0.98	0.83	0.90			
	F4	3ions	0.86	F4	NOx	0.79	F4	COA	0.97	0.98	0.83	0.90	F4	HOA	0.96	0.99	0.92	0.99			
	F5	NO3	0.37				F5	SVOOA	0.84	0.99	0.61	0.94									
	F6	NO3	0.49				F6	SVOOA	0.88	0.97	0.65	0.79									
	F7	NOx	0.79				F7	HOA	0.96	0.99	0.92	0.99									
Summer, 201109	F1	SO4	0.51	F1	SO4	0.65	F1	LVOOA	0.96	0.89	0.93	0.53	F1	LVOOA	0.97	0.95	0.95	0.78			
	F2	SO4	0.39	F2	NO3	0.76	F2	LVOOA	0.97	0.98	0.95	0.94	F2	SVOOA	0.96	0.98	0.88	0.77			
	F3	NO3	0.24	F3	COA_3ions	0.89	F3	SVOOA	0.94	0.94	0.78	0.64	F3	COA	0.98	0.99	0.84	0.92			
	F4	3ions	0.89	F4	NOx	0.83	F4	COA	0.98	0.99	0.84	0.92	F4	HOA	0.82	0.99	0.72	0.98			
	F5	NO3	0.89				F5	SVOOA	0.98	0.97	0.87	0.79									
	F6	NO3	0.54				F6	SVOOA	0.89	0.93	0.85	0.66									
	F7	NOx	0.83				F7	HOA	0.82	0.99	0.72	0.98									
Autumn, 201111	F1	SO4	0.76	F1	SO4	0.80	F1	LVOOA	0.97	0.98	0.96	0.91	F1	LVOOA	0.98	0.96	0.95	0.80			
	F2	3ions	0.81	F2	NO3	0.72	F2	COA	0.98	0.99	0.85	0.92	F2	SVOOA	0.96	0.95	0.89	0.75			
	F3	SO4	0.49	F3	COA_3ions	0.81	F3	LVOOA	0.97	0.90	0.95	0.78	F3	COA	0.98	0.99	0.95	0.92			
	F4	NO3	0.67	F4	NOx	0.64	F4	SVOOA	0.96	0.93	0.83	0.64	F4	HOA	0.99	0.99	0.96	0.98			
	F5	NO3	-0.04				F5	SVOOA	0.94	0.92	0.84	0.69									
	F6	SO4	0.46				F6	LVOOA	0.96	0.91	0.92	0.65									
	F7	NO3	0.10				F7	SVOOA	0.93	0.95	0.89	0.81									
	F8	NOx	0.64				F8	HOA	0.99	0.99	0.96	0.98									
Winter, 201202	F1	SO4	0.65	F1	SO4	0.80	F1	LVOOA	0.97	0.98	0.96	0.97	F1	LVOOA	0.99	0.95	0.98	0.92			
	F2	NO3	0.26	F2	NO3	0.55	F2	SVOOA	0.90	0.93	0.81	0.83	F2	SVOOA	0.96	0.96	0.88	0.82			
	F3	NO3	0.38	F3	COA_3ions	0.87	F3	SVOOA	0.97	0.98	0.88	0.79	F3	COA	0.98	0.99	0.90	0.92			
	F4	SO4	-0.06	F4	NOx	0.56	F4	LVOOA	0.97	0.91	0.96	0.89	F4	HOA	0.99	0.99	0.96	0.98			
	F5	SO4	0.50				F5	LVOOA	0.99	0.91	0.99	0.79									
	F6	3ions	0.87				F6	COA	0.98	0.99	0.90	0.92									
	F7	NOx	0.56				F7	HOA	0.99	0.99	0.96	0.98									

Table S4 Elemental analysis for the four factors in four seasons.

	HOA				COA				SVOOA				LVOOA			
	OM/OC	O/C	H/C	N/C	OM/OC	O/C	H/C	N/C	OM/OC	O/C	H/C	N/C	OM/OC	O/C	H/C	N/C
Spr., 201105	1.27	0.09	1.67	0.01	1.25	0.08	1.74	0.01	1.47	0.23	1.46	0.02	2.08	0.68	1.13	0.06
Sum., 201109	1.49	0.25	1.67	0.01	1.29	0.11	1.69	0.01	1.74	0.42	1.38	0.05	2.26	0.79	1.30	0.08
Aut., 201111	1.27	0.08	1.76	0.01	1.28	0.10	1.69	0.01	1.65	0.36	1.44	0.04	1.97	0.60	1.27	0.05
Win., 201202	1.28	0.09	1.77	0.01	1.30	0.12	1.66	0.01	1.53	0.27	1.48	0.04	1.98	0.63	1.25	0.02

6. Back trajectory analysis evaluation

The clustering of trajectories is based on the total spatial variance (TSV) method (Draxler et al., 2012). This method minimizes the intra-cluster differences among trajectories while maximizing the inter-cluster differences.

In the clustering process, the spatial variance (SV, the squared distances between the endpoints of the cluster's component trajectories and the mean of the trajectories in that cluster), the cluster spatial variance (CSV, the sum of the SVs of all trajectories within the cluster), and the total spatial variance (TSV, the sum of the CSVs for all clusters) are calculated.

Initially, both CSV and TSV are zero, with each trajectory being defined to be a cluster, which means that there are N trajectories and N clusters. The clustering involves combination of two clusters with the lowest increase in TSV. In the first iteration, the two clusters that result in the lowest increase in TSV are combined. Then, the number of clusters reduced to N-1, with one cluster consisting of two trajectories and the others consisting of one. The process continues until the last two clusters are merged, resulting in N trajectories in one cluster.

In the first few iterations, the TSV increases dramatically, then gradually levels off and lifts again by the end of calculation. The final increase happens when disparate clusters start to be merged, indicating that the paired clusters are no longer similar. The ideal final number of clusters is just before the inflection point where the final rise occurs.

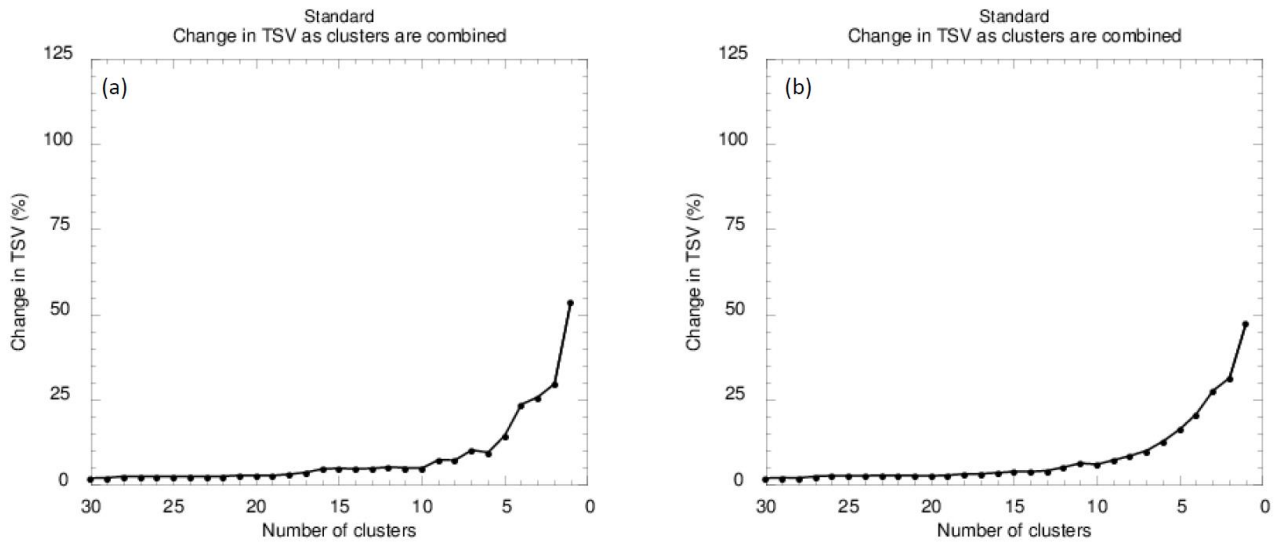

Figure S18 Total spatial variance (TSV) as a function of number of clusters for (a) 300 m and (b) arrival heights.

Figure S18 shows the changes in total spatial variance (TSV) as a function of number of clusters for 300 m arrival height (left) and for 500 m arrival height (right). For both case, the changes in TSV decreased substantially from 4 to 6 cluster solutions. Therefore, solutions (shown in Figure S19) with 4, 5, and 6 clusters for both arrival heights were obtained and subject to further evaluation.

Species concentrations of distinct sources as indicators of (a) transported species (sulfate and LVOOA) and (b) locally emitted species (HOA and COA) were used for the evaluation. The concentrations of these four species in each cluster are plotted in box-whisker plots as shown in Figures S20 and S21 for 300 m and 500 m arrival height, respectively. The evaluation rationale is as follows: (1) a larger number of clusters can potentially provide more detailed information and should be

attempted; (2) too many clusters may be purely mathematical and make little physical sense, thus should be avoided if it is the case; (3) transported species with anthropogenic origins should be associated with long trajectories from the continent; (4) locally emitted species should be associated with short trajectories with calm wind. The optimal number of clusters balancing points (1) and (2) is chosen with an evaluation of points (3) and (4) for the same arrival height. A similar evaluation using points (3) and (4) is employed to choose a final solution from the optimal solutions at each arrival height.

As shown in Figure S19 (a) to (c), going from the 4-cluster solution to the 5-cluster solution splits Cluster 2 in the 4-cluster solution into Clusters 2 and 5 in the 5-cluster solution, while going from the 5-cluster solution to the 6-cluster solution splits Cluster 3 into Clusters 3 and 5 in the 6-cluster solution. In Figure S20, the split of Cluster 2 in the 4-cluster solution into Cluster 2 and 5 in the 5-cluster solution leads to slightly higher SO4 and LVOOA in Cluster 5 than in Cluster 2 in the 5-cluster solution, while to substantially lower HOA and COA in Cluster 5 than in Cluster 2 in the 5-cluster solution. This observation suggests that a split of the otherwise lumped Cluster 2 in the 4-cluster solution can provide consistent interpretation of regional and local pollutants. One the other hand, from panels (b) to panels (c) in Figure S20, the split of Cluster 3 in the 5-cluster solution into Clusters 3 and 5 in the 6-cluster solution does not lead to such consistency. In the 6-cluster solution, SO4 in Cluster 3 is higher than in Cluster 5 (c-1), while LVOOA in Cluster 3 is lower than in Cluster 5 (c-2). Similarly, HOA in Cluster 3 is higher than in Cluster 5 (c-3), while COA in Cluster 3 is lower than in Cluster 5 (c-4). This

observation suggests that going from 5-cluster solution to 6-cluster solution does not provide additional information that is consistent with the tracer species concentrations.

As shown in Figure S19 (d) to (f), going from the 4-cluster solution to the 5-cluster solution splits Cluster 1 in the 4-cluster solution into Clusters 1 and 2 in the 5-cluster solution, while going from the 5-cluster solution to the 6-cluster solution splits Cluster 2 into Clusters 2 and 3 in the 6-cluster solution. In Figure S21, the split of Cluster 1 in the 4-cluster solution to Clusters 1 and 2 in the 5-cluster solution leads to lower concentrations in Cluster 1 and higher concentrations in Cluster 2 for all four species, indicating consistency. On the other hand, the split of Cluster 2 in the 5-cluster solution to Clusters 2 and 3 does not lead to such a consistency. SO4 concentration in Cluster 2 is lower than in Cluster 3, while LVOOA in Cluster 2 is higher than in Cluster 3 in the 6-cluster solution. The effect is less pronounced for HOA but HOA in Cluster 2 is slightly higher than in Cluster 3, while COA in Cluster 2 is much higher than in Cluster 3 in the 6-cluster solution. Therefore, going from 5-cluster solution to 6-cluster solution does not provide consistent interpretation of the tracer species concentrations.

5-cluster solutions from both the arrival heights seems reasonable. The major difference between these two solutions is that the solution from arrival height of 300 m has a short trajectory (Cluster 3) representing the air mass circulating the Pearl River Delta (PRD) region (Figure S19-b, which cannot be captured by setting the arrival height of 500 m (Figure S19-e). Therefore, we choose the 5-cluster solution with arrival height of 300 m for the analysis to reflect the impact of the nearby PRD region.

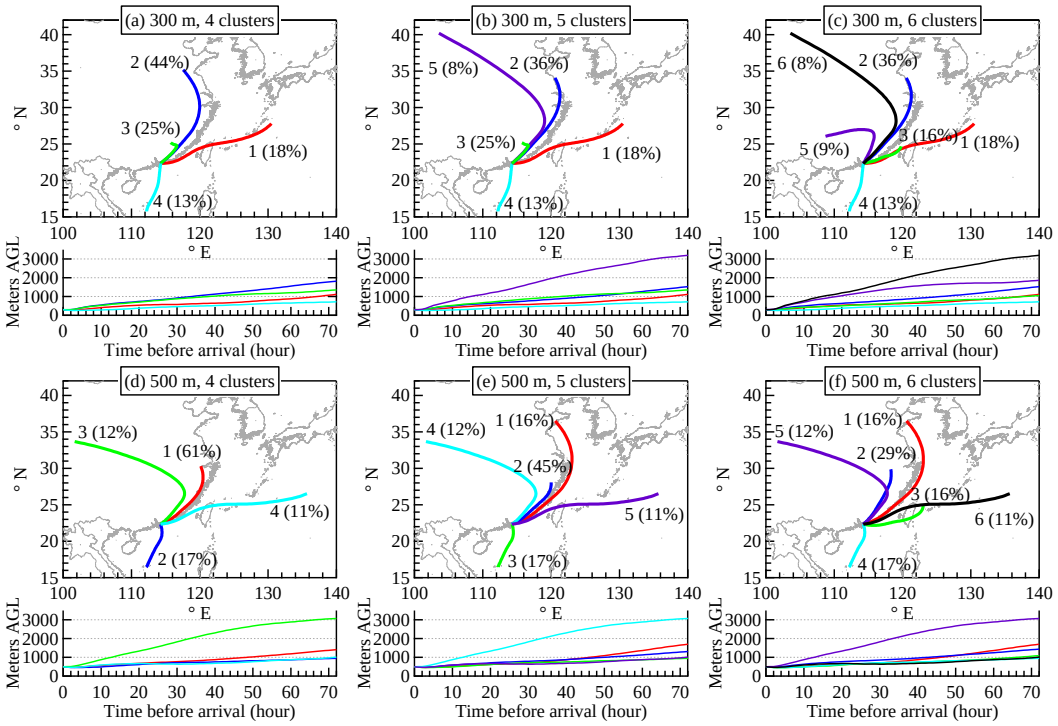

1

2 Figure S19 Solutions with 4 to 6 clusters for arrival height at 300 m (a – c) and 500 m (d – f).

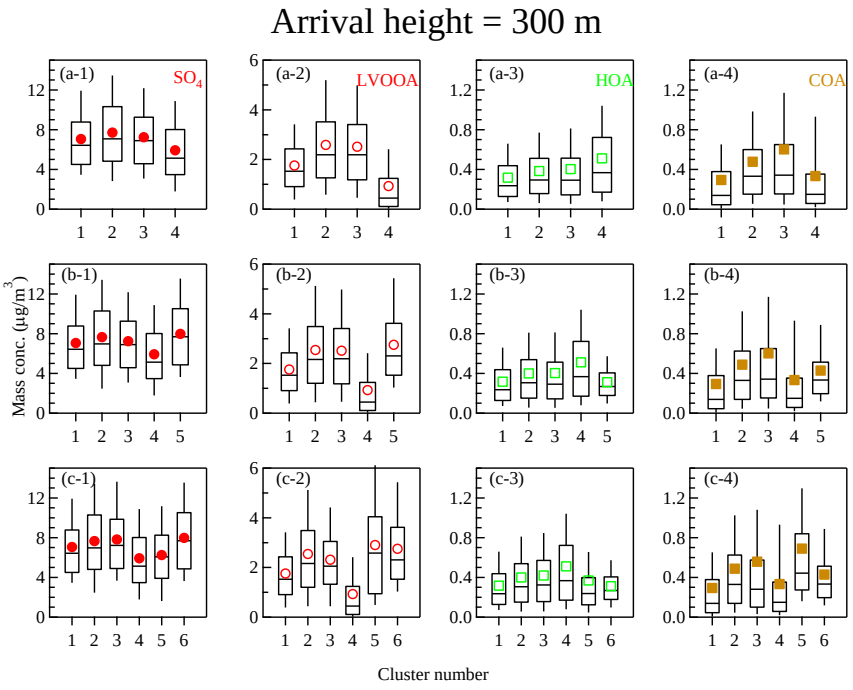

3

4 Figure S20 Mass concentrations of sulfate (a-1, b-1, and c-1), LVOOA (a-2, b-2, and c-2), HOA (a-3,
5 b-3, and c-3), and COA (a-4, b-4, and c-4) for 4-cluster (panels a-1 to a-4), 5-cluster (panels b-1 to b-
6 4), and 6-cluster (panels c-1 to c-4) solutions for arrival height at 300 m.

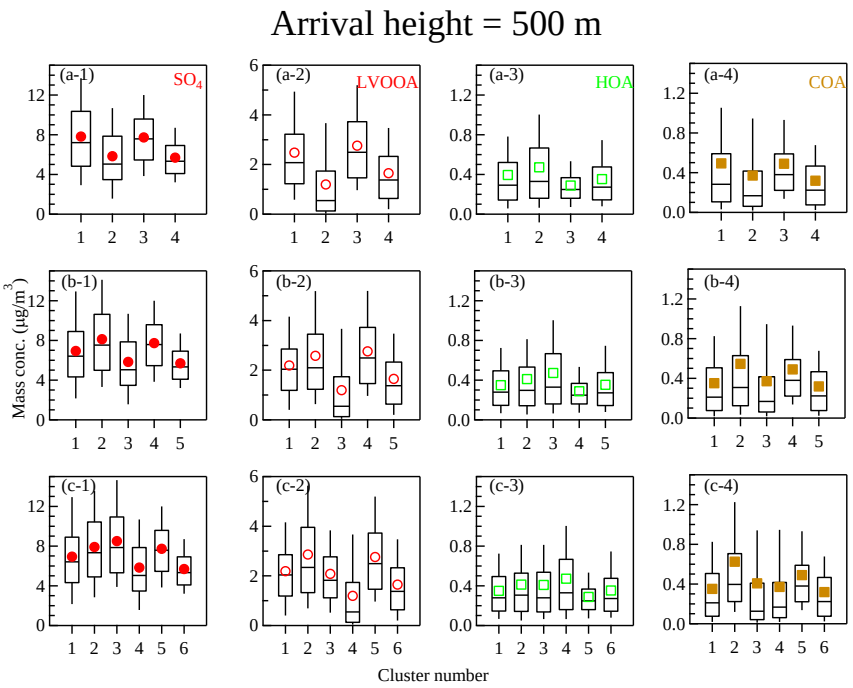

Figure S21 Mass concentrations of sulfate (a-1, b-1, and c-1), LVOOA (a-2, b-2, and c-2), HOA (a-3, b-3, and c-3), and COA (a-4, b-4, and c-4) for 4-cluster (panels a-1 to a-4), 5-cluster (panels b-1 to b-4), and 6-cluster (panels c-1 to c-4) solutions for arrival height at 500 m.

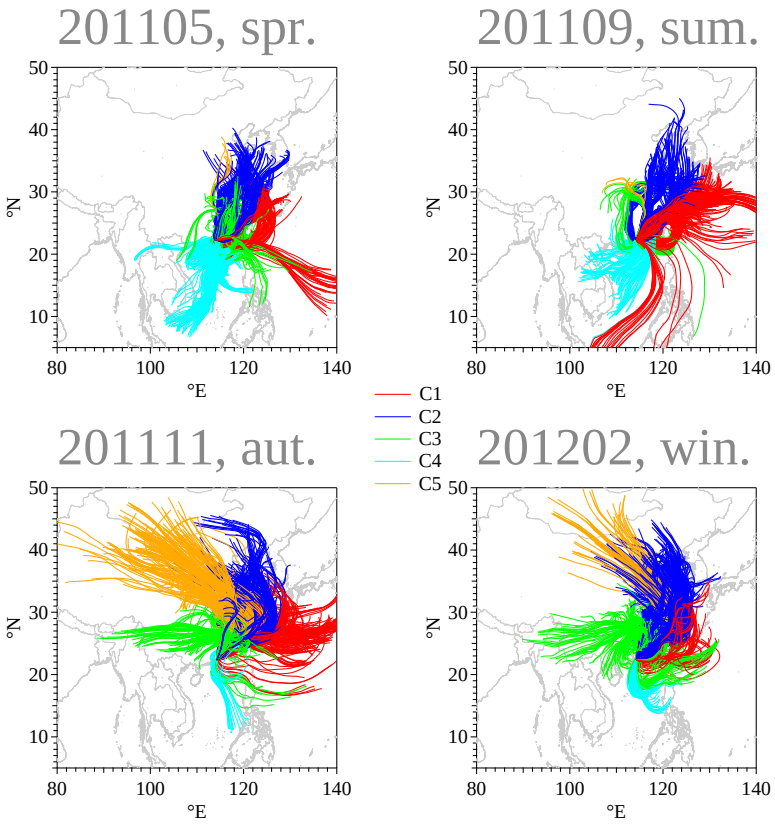

Figure S22 Individual trajectories in each measurement month colored coded by clusters. The individual trajectories are from the 5-cluster solution with an arrival height of 300 m.

7. Reference

Bahreini, R., Jimenez, J. L., Wang, J., Flagan, R. C., Seinfeld, J. H., Jayne, J. T., and Worsnop, D. R.: Aircraft-based aerosol size and composition measurements during ACE-Asia using an Aerodyne aerosol mass spectrometer, J. Geophys. Res.-Atmos., 108, 10.1029/2002jd003226, 2003.

Collier, S., and Zhang, Q.: Gas-Phase CO2 Subtraction for Improved Measurements of the Organic Aerosol Mass Concentration and Oxidation Degree by an Aerosol Mass Spectrometer, Environ. Sci. Technol., 47, 14324-14331, 2013.

DeCarlo, P. F., Slowik, J. G., Worsnop, D. R., Davidovits, P., and Jimenez, J. L.: Particle morphology and density characterization by combined mobility and aerodynamic diameter measurements. Part 1: Theory, Aerosol Sci. Technol., 38, 1185-1205, 2004.

DeCarlo, P. F., Kimmel, J. R., Trimborn, A., Northway, M. J., Jayne, J. T., Aiken, A. C., Gonin, M., Fuhrer, K., Horvath, T., Docherty, K. S., Worsnop, D. R., and Jimenez, J. L.: Field-deployable, high-resolution, time-of-flight aerosol mass spectrometer, Anal. Chem., 78, 8281-8289, 2006.

Gong, Z. H., Lan, Z. J., Xue, L., Zeng, L. W., He, L. Y., and Huang, X. F.: Characterization of submicron aerosols in the urban outflow of the central Pearl River Delta region of China, Front. Env. Sci. Eng., 6, 725-733, 2012.

Gunthe, S. S., Rose, D., Su, H., Garland, R. M., Achtert, P., Nowak, A., Wiedensohler, A., Kuwata, M., Takegawa, N., Kondo, Y., Hu, M., Shao, M., Zhu, T., Andreae, M. O., and Poschl, U.: Cloud condensation nuclei (CCN) from fresh and aged air pollution in the megacity region of Beijing, Atmos. Chem. Phys., 11, 11023-11039, 2011.

Han, Y. M., Iwamoto, Y., Nakayama, T., Kawamura, K., and Mochida, M.: Formation and evolution of biogenic secondary organic aerosol over a forest site in Japan, J. Geophys. Res.-Atmos., 119, 259-273, 2014.

He, L. Y., Huang, X. F., Xue, L., Hu, M., Lin, Y., Zheng, J., Zhang, R. Y., and Zhang, Y. H.: Submicron aerosol analysis and organic source apportionment in an urban atmosphere in Pearl River Delta of China using high-resolution aerosol mass spectrometry, J. Geophys. Res.-Atmos., 116, Artn D12304, DOI: 10.1029/2010JD014566, 2011.

Hu, W. W., Hu, M., Yuan, B., Jimenez, J. L., Tang, Q., Peng, J. F., Hu, W., Shao, M., Wang, M., Zeng, L. M., Wu, Y. S., Gong, Z. H., Huang, X. F., and He, L. Y.: Insights on organic aerosol aging and the influence of coal combustion at a regional receptor site of central eastern China, Atmos. Chem. Phys., 13, 10095-10112, 2013.

Huang, X. F., He, L. Y., Hu, M., Canagaratna, M. R., Sun, Y., Zhang, Q., Zhu, T., Xue, L., Zeng, L. W., Liu, X. G., Zhang, Y. H., Jayne, J. T., Ng, N. L., and Worsnop, D. R.: Highly time-resolved chemical characterization of atmospheric submicron particles during 2008 Beijing Olympic Games using an Aerodyne High-Resolution Aerosol Mass Spectrometer, Atmos.

Chem. Phys., 10, 8933-8945, 2010.
Huang, X. F., He, L. Y., Hu, M., Canagaratna, M. R., Kroll, J. H., Ng, N. L., Zhang, Y. H., Lin, Y., Xue, L., Sun, T. L., Liu, X. G., Shao, M., Jayne, J. T., and Worsnop, D. R.: Characterization of submicron aerosols at a rural site in Pearl River Delta of China using an Aerodyne High-Resolution Aerosol Mass Spectrometer, Atmos. Chem. Phys., 11, 1865-1877, 2011.
Huang, X. F., He, L. Y., Xue, L., Sun, T. L., Zeng, L. W., Gong, Z. H., Hu, M., and Zhu, T.: Highly time-resolved chemical characterization of atmospheric fine particles during 2010 Shanghai World Expo, Atmos. Chem. Phys., 12, 4897-4907, 2012.
Huang, X. F., Xue, L., Tian, X. D., Shao, W. W., Sun, T. L., Gong, Z. H., Ju, W. W., Jiang, B., Hu, M., and He, L. Y.: Highly time-resolved carbonaceous aerosol characterization in Yangtze River Delta of China: Composition, mixing state and secondary formation, Atmos. Environ., 64, 200-207, 2013.
Park, K., Park, J., Lee, S., Cho, H. J., and Kang, M.: Real time measurement of chemical composition of submicrometer aerosols at urban Gwangju in Korea by aerosol mass spectrometer, Atmos. Environ., 62, 281-290, 2012.
Setyan, A., Zhang, Q., Merkel, M., Knighton, W. B., Sun, Y., Song, C., Shilling, J. E., Onasch, T. B., Herndon, S. C., Worsnop, D. R., Fast, J. D., Zaveri, R. A., Berg, L. K., Wiedensohler, A., Flowers, B. A., Dubey, M. K., and Subramanian, R.: Characterization of submicron particles influenced by mixed biogenic and anthropogenic emissions using high-resolution aerosol mass spectrometry: results from CARES, Atmos. Chem. Phys., 12, 8131-8156, 2012.
Sun, J. Y., Zhang, Q., Canagaratna, M. R., Zhang, Y. M., Ng, N. L., Sun, Y. L., Jayne, J. T., Zhang, X. C., Zhang, X. Y., and Worsnop, D. R.: Highly time- and size-resolved characterization of submicron aerosol particles in Beijing using an Aerodyne Aerosol Mass Spectrometer, Atmos. Environ., 44, 131-140, 2010.
Sun, Y. L., Wang, Z. F., Dong, H. B., Yang, T., Li, J., Pan, X. L., Chen, P., and Jayne, J. T.: Characterization of summer organic and inorganic aerosols in Beijing, China with an Aerosol Chemical Speciation Monitor, Atmos. Environ., 51, 250-259, 2012.
Sun, Y. L., Wang, Z. F., Fu, P. Q., Jiang, Q., Yang, T., Li, J., and Ge, X. L.: The impact of relative humidity on aerosol composition and evolution processes during wintertime in Beijing, China, Atmos. Environ., 77, 927-934, 2013.
Takami, A., Miyoshi, T., Shimono, A., and Hatakeyama, S.: Chemical composition of fine aerosol measured by AMS at Fukue Island, Japan during APEX period, Atmos. Environ., 39, 4913-4924, 2005.
Takami, A., Miyoshi, T., Shimono, A., Kaneyasu, N., Kato, S., Kajii, Y., and Hatakeyama, S.: Transport of anthropogenic aerosols from Asia and subsequent chemical transformation, J. Geophys. Res.-Atmos., 112, 2007.
Takegawa, N., Miyakawa, T., Kondo, Y., Jimenez, J. L., Zhang, Q., Worsnop, D. R., and Fukuda, M.: Seasonal and diurnal variations of submicron organic aerosol in Tokyo observed using the

Aerodyne aerosol mass spectrometer, J. Geophys. Res.-Atmos., 111, 2006.
Topping, D., Coe, H., McFiggans, G., Burgess, R., Allan, J., Alfarra, M. R., Bower, K., Choularton, T. W., Decesari, S., and Facchini, M. C.: Aerosol chemical characteristics from sampling conducted on the Island of Jeju, Korea during ACE Asia, Atmos. Environ., 38, 2111-2123, 2004.
Xiao, R., Takegawa, N., Zheng, M., Kondo, Y., Miyazaki, Y., Miyakawa, T., Hu, M., Shao, M., Zeng, L., Gong, Y., Lu, K., Deng, Z., Zhao, Y., and Zhang, Y. H.: Characterization and source apportionment of submicron aerosol with aerosol mass spectrometer during the PRIDE-PRD 2006 campaign, Atmos. Chem. Phys., 11, 6911-6929, 2011.
Zhang, J. K., Sun, Y., Liu, Z. R., Ji, D. S., Hu, B., Liu, Q., and Wang, Y. S.: Characterization of submicron aerosols during a month of serious pollution in Beijing, 2013, Atmos. Chem. Phys., 14, 2887-2903, 2014.
Zhang, Q., Meng, J., Quan, J., Gao, Y., Zhao, D., Chen, P., and He, H.: Impact of aerosol composition on cloud condensation nuclei activity, Atmos. Chem. Phys., 12, 3783-3790, 2012.